POLITECNICO DI TORINO

Master's Degree in Mechatronic engineering

Master's Degree Thesis

Design and Implementation of a Hybrid Localization Algorithm for Autonomous Navigation Systems

Supervisors

Prof. Michele TARAGNA

Ing. Francesco SOTTILE

Candidate

Giuseppe LUPO

April 2022

Abstract

Recently, autonomous navigation in indoor environments has received increasing attention from the research community. In fact, different autonomous systems such as UAVs are going to be adopted also in these environments to support various applications, for instance, for logistic operations to perform some inspection and monitoring tasks in industrial plants as well as in greenhouses. In these scenarios, it is fundamental to know not only the target's position but also its attitude. Regarding the position estimation, usually the Ultra-Wideband (UWB) technology is employed providing accurate Time of Arrival (ToA) measurements while for the attitude estimation, Inertial Measurement Units (IMU) sensors are typically used allowing to estimate roll and pitch of the UAV. However, the estimation of the yaw angle employing a compass sensor is too inaccurate because the Earth's magnetic field in indoor environments is heavily affected by electric and electronic devices as well as surrounding metallic objects and structures. To overcome this limitation, the UWB technology is becoming also a promising solution to estimate the angle with which the transmitted UWB signal arrives at the receiver, thus, exploiting this type of measurement, it is possible to estimate the yaw angle of the target. In particular, the UWB technology can be used to perform Angle of Arrival (AoA) measurements employing antenna arrays at the receiver.

The focus of this thesis is to design different real-time localization solutions for indoor environments based on Ultra-Wideband (UWB) technology that enable autonomous navigation. The UWB technology can be used to perform Time of Arrival (ToA) and Angle of Arrival (AoA) measurements to estimate the position and the orientation of the tag. These measurements can be merged through an Extended Kalman Filter (EKF) to obtain a more accurate estimator. In this thesis after a comprehensive overview of the localization problem, first two localization solution that uses only ToA measurements will be designed and then a hybrid solution that combines ToA and AoA measurements. Lastly, real PDoA and ToA measurements will be presented to analyze real measurement errors.

Table of Contents

List of Tables

List of Figures

Acronyms

UWB
: Ultra-Wideband

UAV
: Unmanned Aerial Vehicle

ToA
: Time of Arrival

AoA
: Angle of Arrival

RSS
: Received Signal Strength

TDoA
: Time Difference of Arrival

EKF
: Extended Kalman Filter

INS
: Inertial Navigation System

IMU
: Inertial Measurement Units

GNSS
: Global Navigation Satellite System

GPS
: Global Positioning System

RFID
: Radio-Frequency Identification

IR
: Infrared

BLE
: Bluetooth Low Energy

Chapter 1

Overview of localization in indoor environments

Over the past few decades, indoor device localization has been extensively studied, mostly in industrial settings and for wireless sensor networks and robotics. A positioning system allows a mobile device to estimate its location and makes that location available for position-based services like navigation and other monitoring and tracking functions. Global Navigation Satellite System (GNSS), such as the Global Positioning System (GPS), are the standard for outdoor localization with a clear sky view. However in indoor environments line-of-sight transmission between receivers and satellites is not possible, thus GPS can not be used. Indoor environments are more complex than outdoor ones. The propagation of electromagnetic waves is influenced by obstacles, such as walls, objects, and people, which create multi-path effects. In fact, the accuracy of positioning is affected by some interference and noise sources from other wired and wireless networks. There are multiple paths and environmental consequences as a result of the building's shape, human motion, and atmospheric conditions.

For location-based applications, location data typically provides absolute, relative, or proximity information. The absolute location information provides an estimate of the position $[x_T, y_T]$ of a target with respect to a map of the locating area that should be available before the estimation of the position. The relative location information is measured with respect to a reference node and gives an estimate of the distance. To determine the position of a target at least three relative measures are necessary. The last type of position data is the proximity location information which specifies an area where a target is. When a tracked target is detected by a detector, the position of the target is considered to be in the proximity area centered in the detector location but this technique can not give absolute position estimations. In [1][2][3] different indoor ranging techniques are described, such as Received Signal Strength (RSS), Time of Arrival (ToA), Time Difference of Arrival (TDoA), Angle of Arrival (AoA). These solutions rely on radio communication technologies, such as WiFi, Bluetooth, Radio-Frequency Identification (RFID), Ultra-Wideband (UWB), Infrared (IR), acoustic sounds and ultrasounds. In [3] the four main techniques for indoor localization are presented: triangulation, fingerprinting, vision analysis and proximity. Except for the last one, all these strategies can provide absolute location.

- **Triangulation**, if the coordinates of three reference nodes are known, measures the absolute location of a target by using the three lengths or directions of the distances between the target and the reference nodes. To calculate these distances can be used the RSS, the AoA or the ToA.
- **Fingerprinting** positioning technique is proposed to increase the accuracy of indoor position measurements by acquiring first location-related data (generally RSSI) of the location estimation area in the offline training phase and then during the online position determination phase, the location of a target object is measured and compared with the data collected in the first phase.
- The **vision analysis** estimates a location from the image received by one or multiple points. Since no additional tracked devices must be carried by the tracked persons, vision positioning provides comfort and efficiency to users.
- **Proximity** positioning techniques can not estimate with high accuracy the target position but specify only if a target is in a proximity area or not.

1.1 Ranging techniques

1.1.1 Received Signal Strength (RSS)

The RSS is one of the simplest approaches for indoor localization. Generally measured in decibel-milliwatts (dBm) or milliWatts (mW), the RSS is the actual signal power strength received at the receiver. A transmitter (Tx) and a receiver (Rx) device's distance can be estimated using the RSS; the greater the RSS value, the smaller the distance is between Tx and Rx. With the knowledge of the transmission power or the power at the reference location, the distance can be estimated using a variety of different signal propagation models. RSS indicator, or RSSI, is a relative RSS measurement with arbitrary units that is usually specified by each chip maker.

$$RSSI = A - 10nlog_{10}(d) \tag{1.1}$$

Where A is the RSSI value at a reference distance from the receiver and n is the path loss exponent (which varies from 2 in free space to 4 in indoor environments).

The RSSI and a straightforward path-loss propagation model can be used to estimate the distance d between Tx and Rx as:

$$d = 10^{\left(\frac{A-RSSI}{10n}\right)} \tag{1.2}$$

The RSS-based approach is simple and cost-efficient but suffers from poor localization accuracy due to additional signal attenuation resulting from transmission through big obstacles and RSS fluctuation due to multipath fading and indoor noise. It is not likely to obtain high localization accuracy without using complex algorithms but to mitigate these effects, a variety of filters or averaging mechanisms can be used.

1.1.2 Time of Arrival (ToA)

Time of Arrival (ToA) or Time of Flight (ToF) is the measured signal propagation time at which a signal first arrives at the receiver Rx from the transmitter Tx. The distance between Tx and Rx can be calculated by multiplying the ToA value by the speed of light, $c = 3 \cdot 10^8$ m/s.

$$D_{ij} = (t_2 - t_1) \cdot c \tag{1.3}$$

Where t_1 is the time at which the TX_i sends a message to the RX_j and t_2 is the time at which the RX receives the message. ToA estimation accuracy mainly depends on the signal bandwidth and the sampling rate. A larger bandwidth increases the resolution of the ToA estimation in a multipath indoor environment as well as a low sampling rate reduces the ToA resolution since the signal may arrive between the sampled intervals.

1.1.3 Time Difference of Arrival (TDoA)

Differently from the ToA where the absolute signal propagation time is measured, Time Difference of Arrival (TDoA) uses the difference in signal propagation time from different transmitters, measured at the receiver. Multiplying the TDoA measurements τ_{ij} by the speed of light we obtain physical distance measurements.

$$d_{ij} = d_i - d_j = c \cdot \tau_{ij} \tag{1.4}$$

Where τ_{ij} is the TDoA measured at the receiver RX from a pair of Transmitters TX_i and TX_j, d_i is the distance between the RX and TX_i.

The ranging measurement d_{ij} is the difference of the distance of the transmitters from the receiver and defines a hyperboloid where the receiver is located as shown in the equation (2.19).

$$d_{ij} = \sqrt{(X_i - x)^2 + (Y_i - y)^2 + (Z_i - z)^2} - \sqrt{(X_j - x)^2 + (Y_j - y)^2 + (Z_j - z)^2} \tag{1.5}$$

Where (X_i, Y_i, Z_i) and (X_j, Y_j, Z_j) are the coordinates of the transmitters and (x,y,z) are the coordinates of the receiver to be estimated. In 1.1 is shown the TDOA measurement configuration.

The receiver position is estimated as the intersection of three hyperboloids, thus at least the TDoA measurements from three different transmitters are needed. It is possible to solve the system of hyperbola equations using either Taylor-series expansion or linear regression. TDoA approach requires strict synchronization but only between transmitters contrary to the TOA approach that requires synchronization between transmitter and receiver. TDoA measurement accuracy is affected mainly by the signal bandwidth, the signal rate at the receiver and the presence of a direct line of sight between the transmitters and the receiver.

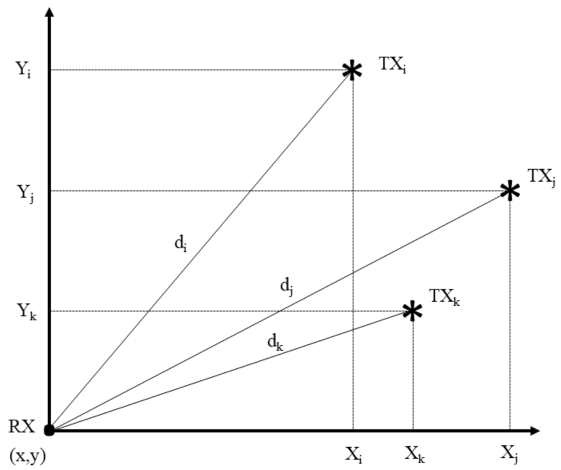

Figure 1.1: TDOA measurement configuration

1.1.4 Angle of Arrival (AoA)

The Angle of Arrival (AoA) gives an estimate of the angle of rotation of the object to be tracked with respect to a reference node. This approach requires an antenna array at the receiver since AoA is based on the calculation of the phase difference α of a single signal received at two different antennas. The distance d between two antennas is chosen to be less than half the signal's wavelength λ. The receivers receive the signal with a path difference p ranging from 0 to d that can be obtained from the phase difference α as

$$p = \frac{\alpha \cdot \lambda}{2\pi} \tag{1.6}$$

Based on the path difference p we can calculate the angle of rotation of the receiver as:

$$\theta = \arcsin \frac{p}{d_{ANTENNA}} \tag{1.7}$$

In 1.2 is shown the AOA measurement configuration.

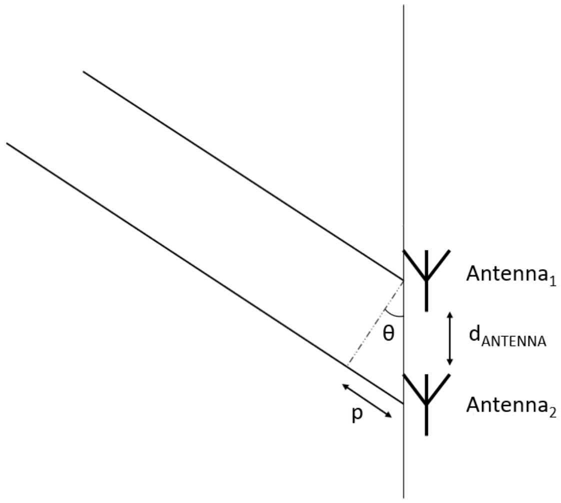

Figure 1.2: AOA measurement configuration.

1.2 Localization Technologies

In this section, the mostly used localization technologies are presented. This section presents the main localization technologies. Radio-frequency Positioning systems are described in more detail because they are the most widely used.

- **Infrared (IR) Positioning Systems**
  Different positioning systems based on Infrared (IR) were proposed in the past [4][5]. IR-based positioning systems provide a very accurate position estimation, though have some limitation that makes them not really suitable for positioning systems. In fact, they need a direct line of sight between transmitter and receiver and strong light sources interfere with communication. Moreover, although the IR emitters are cheap, the whole positioning system is expensive.

- **Ultra-sound Positioning Systems**
  In ultra-sound positioning systems [6] distances are mainly calculated by measuring the ToA of ultrasound signals (>20 KHz). Differently from RF

signals, the sound velocity varies significantly depending on humidity and temperature condition, thus temperature sensors are often deployed to take into account these changes. Usually ultrasound signals are combined with RF signals, which are required for synchronization.

- **Vision-Based Positioning Systems**
  In vision-based positioning systems [7], a low price camera can cover a large area to track the location of a target or to identify persons through image processing algorithms in a complex indoor environment. This technology increases the comfort of the tracked person, because it is not necessary to carry any device but does not guarantee people's privacy. The position estimations are based on images saved in a database that needs to be updated due to changes in the environment. For this reason, this method suffers in dynamic environments that change rapidly.

- **Audible Sound Positioning System**
  Acoustic signal-based positioning systems [8] work by transmitting modulated acoustic signals containing some time-related information such as time stamps, that are received by a microphone sensor for ToA estimation. The transmitted power should be kept low enough to prevent noise pollution and to increase low power detection at the receiver, sophisticated signal processing methods are required.

- **Radio-Frequency Positioning Systems**
  Since radio waves have the advantage to travel through the walls and human bodies easier, positioning systems based on this kind of signal have a larger coverage area and require less hardware with respect to the other systems presented before. Technologies such as RFID, WiFi, Bluetooth and UWB are the most used radio-frequency positioning systems and are described in detail in the following paragraphs.

1.2.1 Radio-Frequency Identification (RFID)

RFID (RF Identification) is a means of storing and retrieving data through electromagnetic transmission. An RFID system consists of a reader that can communicate with RFID tags [9]. Each reader has a pre-determined power level, thus defining a certain range in which it can detect RFID tags. RFID systems can be either active or passive depending on whether the tags include an internal power source or are powered only by the electromagnetic energy transmitted from the RFID reader. By properly placing the readers in known locations, the whole region can be divided into a number of sub-regions, where each sub-region can be uniquely identified by the subset of readers that cover that subregion. The range measurements are impacted by a variety of factors, including both static obstacles and dynamic human movement. Even a static object could occasionally be recorded in multiple sub-regions as a result of these dynamic interferences. To overcome these issues, in [10] it is suggested to include additional fixed location reference tags to help location calibration. Since the reference tags are sensitive to the same environmental effects as the tags to be identified, this method helps counteract many environmental influences that cause fluctuations in the detected range.

1.2.2 WiFi

The IEEE 802.11 standard, also referred to as WiFi, is primarily used to provide networking capabilities and Internet connections to various devices. However, since existing WiFi access points can also be used as reference points for signal collection, simple localization systems can be built without the need for additional infrastructure, reducing the cost of positioning services. Efficient algorithms are required to improve localization accuracy because existing WiFi networks are not deployed for localization purposes but to maximize data throughput and network coverage for communication purposes. WiFi-based localization systems can use different ranging techniques, although Received Signal Strength (RSS) is the most common, often used in conjunction with fingerprinting algorithms as in the COMPASS system [11]. Usually a radio map of an indoor area is constructed to model RSS values at predefined reference points and then a tag position can be determined in real-time using the model and the current WiFi signal values.

1.2.3 Bluetooth

Bluetooth consists of the MAC and physical layer specifications for connecting wireless devices in a particular area [1]. Bluetooth chipsets are low cost and in addition allow the reuse of Bluetooth-enabled devices when used for location sensing since Bluetooth technology has been implanted in various types of devices. However, The system can only give precision from 2 to 3 meters away with a latency of roughly 20 seconds, which is a drawback of bluetooth-based locating systems. The more advanced versions of Bluetooth, such as Bluetooth Low Energy (BLE) can be used with different localization techniques such as RSS, AoA and ToA, but the first is certainly the most used. iBeacons (by Apple Inc.) [12] and Eddystone (by Google Inc.) [13] are two BLE-based protocols that have been proposed for context aware proximity based services. Any BLE-enabled device with a dedicated application for listening to beacons can pick up the beacon messages and use RSSI to determine how close the beacon device is to the user. In the case of iBeacon [12], based on the strength of the RSSI, the user is classified in immediate (<1m), near (1-3m), far(>3m) and unknown regions.

1.2.4 Ultra-Wideband (UWB)

The Ultra-Wideband(UWB) was initially developed and extensively used for military purposes and was not used for commercial communication until the U.S. Federal Communications Commission (FCC) permitted the use of unlicensed UWB communications. Firstly UWB was used in the context of short-range, high data rate communications in personal area networks (PANs), but recently has emerged as a prominent technology for indoor localization that can react a centimeter accuracy [14]. In UWB, pulses which have a short duration ($<$ 1ns), are transmitted in the frequency range from 3.1 to 10.6 GHz over a large bandwidth ($>$500 MHz) [1]. UWB sensors are cheap and provide a high data rate, making them an efficient solution in terms of costs. The very short duration of UWB pulses allows to filter the reflected signals from the main signal, making them less sensitive to multi-path distortion of radio signals reflected by walls in indoor environments differently from other RF positioning systems that suffer on this aspect and in many cases need complex time delay estimation algorithms. Furthermore, the large bandwidth decreases the small-scale fading and the power spectral density, which in conjunction with having a big difference in the radio spectrum with respect to most of the other signals, reduces interference to other systems and the possibility of interception. However, due to the short duration of UWB pulses, clock jitter and drifts in the target and the reference nodes have an impact on the estimation. In UWB communication, in addition to the multipath effect, both multiple access interference (MAI) and non-line-of-sight (NLOS) propagation are a source of error. MAI happens when signals from other nodes interfere with the signal of a given node and can be alleviated using different time slots to transmit from different nodes. Instead, when there is no direct LOS between two nodes, the receiving node is reached only from reflections of the original UWB pulse, thus accurate localization is impossible without any information about NLOS errors. In these cases, some pattern recognition techniques can be adopted but in real systems, it is usually possible to obtain some statistical information about the NLOS error. Using Kalman filters, it is possible to precisely estimate the location of a mobile user in a wireless system.

1.3 Comparative analysis of different localization systems

The presented localization technologies can be compared under different aspects, although some features such as the cost and the complexity can vary widely depending on the specific requirements of the application and the level of accuracy required. However, for a general discussion a comparative table is presented.

Positioning system	**Maximum Range**	**Power Consumption**	**Accuracy**	**Limitations**
RFID-based	10 m	Low	2-3 m	Inaccurate. Need numerous infrastructure components installed and maintained
WiFi-based	100 m	Moderate	up to 1 m	Not very accurate
Bluetooth-based	70-100 m	Low	2-3 m	Inaccurate. The delay of calculating the position of a tag is long (10s-30s)
Ultra-Wideband-based	20-30 m	Moderate	Tens of centimeters	Short range. Require infrastructure
Infrared-based	Few meters	Low	Few Millimeters	Line of sight requirement. Influenced by light sources. IR waves can not penetrate walls.
Ultrasound-based	Couple-tens of meters	Low-moderate	Centimeter accuracy	Highly influenced from reflected ultrasound signals
Vision-based	Few meters	Low-moderate	Accuracy can not be guaranteed due to multiple interference sources	Not reliable in a dynamic changing environment. People's privacy issues
Audible Sound-based	Couple of meters	Low-Moderate	up to 0.4 cm	Influenced by sound sources in the same place

Table 1.1: Comparison between the proposed localization technologies

Chapter 2

Localization and Orientation Estimation using Extended Kalman Filter

As presented in the previous chapter, the range measurements are influenced by numerous noise sources (mainly NLOS and Multipath Effect). In this chapter, the Extended Kalman Filter (EKF) is proposed as a solution to counteract these effects and to improve the position estimates. A proper choice of the model that represents the system dynamic and the measurements is crucial to obtain good performance by the EKF, thus for this reason different choices for the state model and the measurement model of the system are presented in the following sections. Furthermore, in Appendix A can be found a brief overview of the Extended Kalman Filter.

2.1 State Models for Low Dynamics Scenarios

The formulation of a state model that appropriately describes system dynamics is the first step in the design of the EKF. The models presented are developed for $n = 2$ (2-dimensional), where the parameter $n = 1,2,3$ indicates the space dimension, but can be easily extended to the 3D case.

2.1.1 P Model

The P Model is the most straightforward approach to represent the system dynamics and its state vector is composed only of the target's position coordinates, see equation 2.26. This model practically performs only the Measurement Update because in the Time Update the *a priori* state estimate at each time step equals the *a posteriori* state estimate of the previous time step as can be seen in equation 2.2. The process noise is modeled as an independent random velocity $\tilde{v}$ normally distributed with zero mean and covariance matrix Q_k as a function of the interval of time between two measures Δt_k. The process noise covariance matrix's dimensioning is crucial in the EKF design: low variance values ensure smooth tracking but lengthen settling times of the tracking output.

$$\mathbf{x} = \begin{bmatrix} x & y \end{bmatrix}^T \tag{2.1}$$

$$\hat{\mathbf{x}}_k^- = f(\hat{x}_{k-1}^+, 0) = I_{n \times n} \hat{x}_{k-1}^+ \tag{2.2}$$

$$Q_k = [\Delta t_k I_{n \times n}][\Delta t_k I_{n \times n}]^T \sigma_v^2 \tag{2.3}$$

where σ_v is the standard deviation of a Gaussian distributed velocity vector.

2.1.2 PV Model

The PV Model is a dynamic model that works as long as the target moves at a nearly constant velocity between two adjacent intervals Δt_k. The state vector is composed of the target's position coordinates and velocity components as reported in equation 2.4. A motion with constant speed is described by the transition function in equation 2.5. The covariance matrix Q_k (equation 2.6) of the normally distributed process noise permits us to take into account friction and other forces that might temporally impact the target's dynamics. Again the process noise, modeled in this case as a random acceleration $\tilde{a}$, is a key factor of the design of the EKF. Zero or small variance allows smooth tracking but slows down the filter response and may lead to divergence when the target performs non-linear maneuvers and so the velocity is no longer constant within the interval Δt_k.

$$\mathbf{x} = \begin{bmatrix} x & y & v_x & v_y \end{bmatrix}^T \tag{2.4}$$

$$\hat{\mathbf{x}}_k^- = f(\hat{x}_{k-1}^+, 0) = \begin{bmatrix} I_{n \times n} & \Delta t_k I_{n \times n} \\ 0_{n \times n} & I_{n \times n} \end{bmatrix} \hat{x}_{k-1}^+ \tag{2.5}$$

$$Q_k = \begin{bmatrix} \frac{1}{2} \Delta t_k^2 I_{n \times n} \\ \Delta t_k I_{n \times n} \end{bmatrix} \begin{bmatrix} \frac{1}{2} \Delta t_k^2 I_{n \times n} \\ \Delta t_k I_{n \times n} \end{bmatrix}^T \sigma_a^2 \tag{2.6}$$

where σ_a is the standard deviation of a Gaussian distributed acceleration vector.

2.1.3 PVA Model

PVA Model includes also the acceleration in the state vector, see equation (2.7). In this way, it improves the capability of the filter to track the target during near-constant acceleration maneuvers. However, considering low dynamics scenarios, this model produces no benefit and simpler models provide better performance.

$$\mathbf{x} = \begin{bmatrix} x & y & v_x & v_y & a_x & a_y \end{bmatrix}^T \tag{2.7}$$

$$\hat{\mathbf{x}}_k^- = f(\hat{x}_{k-1}^+, 0) = \begin{bmatrix} I_{n\times n} & \Delta t_k I_{n\times n} & \frac{1}{2}\Delta t_k^2 I_{n\times n} \\ 0_{n\times n} & I_{n\times n} & \Delta t_k I_{n\times n} \\ 0_{n\times n} & 0_{n\times n} & I_{n\times n} \end{bmatrix} \hat{x}_{k-1}^+ \tag{2.8}$$

$$Q_k = \begin{bmatrix} \frac{1}{2}\Delta t_k^2 I_{n\times n} \\ \Delta t_k I_{n\times n} \\ I_{n\times n} \end{bmatrix} \begin{bmatrix} \frac{1}{2}\Delta t_k^2 I_{n\times n} \\ \Delta t_k I_{n\times n} \\ I_{n\times n} \end{bmatrix}^T \sigma_a^2 \tag{2.9}$$

where σ_a is the standard deviation of a Gaussian distributed acceleration vector.

2.2 Measurements Models

The measurement model is a mathematical description of the relationship between the measurements (z) and the state vector (x), as shown in equation 2.10. Measurements and their additive noise are physically referred to a specific coordinate system (often in spherical coordinates) that can differ from the coordinate system that better describes the target motion model. As a result, measurement models in several coordinate systems have been developed. The most popular and natural measurement models are in mixed coordinates, where the target state $\mathbf{x}$ and the process noise are in a reference Cartesian coordinate system, but measurement $\mathbf{z}$ and its additive noise are in the local sensor coordinate system.

$$\mathbf{z}_k = h(\mathbf{x}_k) + \mathbf{v} \tag{2.10}$$

The relation between measurements and process in mixed coordinates is non-linear and a non-linear estimator such as EKF is needed for the position estimation. However, in some cases measurements are directly expressed in the Cartesian reference system, using some sensor systems can happen that the direct measurements are not available or when more localization algorithms referred to the same coordinate system are used sequentially to improve accuracy. For sake of simplicity, the observation models presented in the following are defined according to the P model.

2.2.1 Position Measurements

When position measurements are accessible directly in the same reference coordinate systems used for the state vector (equation 2.11), the measurement equation 2.10 seems to assume a "linear" form according to equation 2.12, but due to non-linear dependency of the noise $\mathbf{v}$ on the state $\mathbf{x}$ this measurement model is in fact non-linear and EKF is still preferable to the classical linear Kalman Filter. The covariance matrix of the measurement noise vector is typically chosen as a $k \times m$ diagonal matrix that has the variances of the component of the measurements as elements, see equation (2.13), where k is the number of components of a single measurement while m is the number of measurements.

$$\mathbf{z} = \begin{bmatrix} x & y \end{bmatrix}^T \tag{2.11}$$

$$h(\hat{\mathbf{x}}_k^-) = I_{n \times n}\, \hat{\mathbf{x}}_k^- \tag{2.12}$$

$$R_k = diag(\begin{bmatrix} \sigma_x^2 & 0 \\ 0 & \sigma_y^2 \end{bmatrix}) \tag{2.13}$$

2.2.2 Distance Measurements

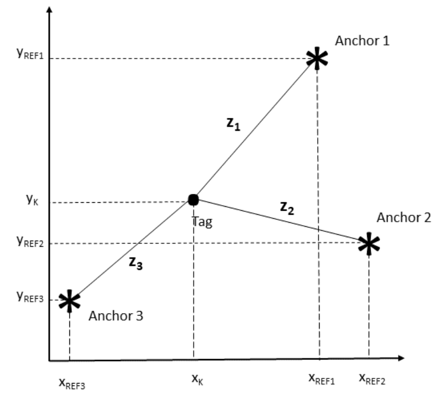

Figure 2.1: Distance measurement model

For many ranging techniques, such as ToA the EKF estimates the target position by processing distance measurements between the target and a set of anchors located at known positions, as can be seen in 2.14. The measurement function $h(x_k)$ is non-linear and looking at the figure 2.1 it is clear that it can be easily defined as the Euclidean distance between the target and the reference nodes (equation 2.15). The Jacobian matrix H_k is computed around the a priori state $\hat{\mathbf{x}}_k^-$ (equation 2.17), since $h(\mathbf{x}_k)$ is non-linear. In equation 2.17 the covariance matrix R_k is a diagonal matrix with the variances of the component of the measurement as elements.

$$\mathbf{z} = \begin{bmatrix} d_{ref1} & d_{ref2} & \dots \end{bmatrix}^T \tag{2.14}$$

$$h(\hat{\mathbf{x}}_k^-) = \begin{bmatrix} \sqrt{(\hat{x}_k^- - x_{ref1,k})^2 + (\hat{y}_k^- - y_{ref1,k})^2} \\ \sqrt{(\hat{x}_k^- - x_{ref2,k})^2 + (\hat{y}_k^- - y_{ref2,k})^2} \\ \vdots \end{bmatrix} \tag{2.15}$$

Where $(x_{ref1,k}, y_{ref1,k})$ are the coordinates of the first anchor

$$H_k = \frac{\partial h}{\partial \mathbf{x}}\bigg|_{\mathbf{x}=\hat{\mathbf{x}}_k^-} = \begin{bmatrix} \frac{\hat{x}_k^- - x_{ref1,k}}{d_{ref1,k}} & \frac{\hat{y}_k^- - y_{ref1,k}}{d_{ref1,k}} & 0 & 0 \\ \frac{\hat{x}_k^- - x_{ref2,k}}{d_{ref2,k}} & \frac{\hat{y}_k^- - y_{ref2,k}}{d_{ref2,k}} & 0 & 0 \\ \vdots & \vdots & \vdots & \vdots \end{bmatrix} \tag{2.16}$$

$$R_k = diag(\begin{bmatrix} \sigma_{dref1}^2 & \sigma_{dref2}^2 & \dots \end{bmatrix}) \tag{2.17}$$

Where $d_{ref1,k} = \sqrt{(\hat{x}_k^- - x_{ref1,k})^2 + (\hat{y}_k^- - y_{ref1,k})^2}$

2.2.3 Angle of Arrival Measurements

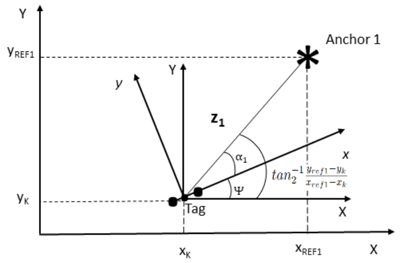

Figure 2.2: AOA measurement model.

For completeness, this paragraph describ a measurement model that estimates the target position processing AoA measurements of the target with respect to some reference nodes (equation 2.18). In order to do that it is necessary to know the rotation angle ψ between the reference frame and the local tag frame where measurements are performed and then $h(\mathbf{x}_k)$ can be obtained from geometrical consideration as shown in Figure 2.2. If the tag is not rotating this angle is constant otherwise if ψ is time-varying, it has to be added to the state vector. AoA measurements can be combined with distance measurements to estimate both target location and orientation since the EKF is a very useful tool to merge different kinds of measurements.

$$\mathbf{z} = \begin{bmatrix} \alpha_1 & \alpha_2 & \dots \end{bmatrix}^T \tag{2.18}$$

$$h(\hat{\mathbf{x}}_k^-) = \begin{bmatrix} tan_2^{-1} \frac{y_{ref1,k} - \hat{y}_k^-}{x_{ref1,k} - \hat{x}_k^-} - \psi \\ tan_2^{-1} \frac{y_{ref2,k} - \hat{y}_k^-}{x_{ref2,k} - \hat{x}_k^-} - \psi \\ \vdots \end{bmatrix} \tag{2.19}$$

Where $(x_{ref1,k}, y_{ref1,k})$ are the coordinates of the first anchor

$$H_k = \frac{\partial h}{\partial x}\bigg|_{\mathbf{x}=\hat{\mathbf{x}}_k^-} = \begin{bmatrix} \frac{-(\hat{y}_k^- - y_{ref1,k})}{(d_{ref1,k})^2} & \frac{(\hat{x}_k^- - x_{ref1,k})}{(d_{ref1,k})^2} \\ \frac{-(\hat{y}_k^- - y_{ref2,k})}{(d_{ref2,k})^2} & \frac{(\hat{x}_k^- - x_{ref2,k})}{(d_{ref2,k})^2} \\ \vdots & \vdots \end{bmatrix} \tag{2.20}$$

$$R_k = diag(\begin{bmatrix} \sigma_{\alpha_1}^2, & \sigma_{\alpha_2}^2, & \dots \end{bmatrix}) \tag{2.21}$$

Where $d_{ref1,k} = \sqrt{(\hat{x}_k^- - x_{ref1,k})^2 + (\hat{y}_k^- - y_{ref1,k})^2}$

2.2.4 Hybrid ToA-AoA Measurements

Considering both ToA and AoA measurements (equation 2.23), it is possible to estimate respectively the localization and the orientation of a target. The EKF is a very useful tool to merge different kinds of measurements, thus is sufficient to add the angle ψ to the state vector (equation 2.22).

$$\mathbf{x} = \begin{bmatrix} x & y & \psi \end{bmatrix}^T \tag{2.22}$$

$$\mathbf{z} = \begin{bmatrix} d_{ref1} & d_{ref2} & \dots & \alpha_1 & \alpha_2 & \dots \end{bmatrix}^T \tag{2.23}$$

$$h(\hat{\mathbf{x}}_k^-) = \begin{bmatrix} \sqrt{(\hat{x}_k^- - x_{ref1,k})^2 + (\hat{y}_k^- - y_{ref1,k})^2} \\ \sqrt{(\hat{x}_k^- - x_{ref2,k})^2 + (\hat{y}_k^- - y_{ref2,k})^2} \\ \vdots \\ tan_2^{-1} \frac{y_{ref1,k} - \hat{y}_k^-}{x_{ref1,k} - \hat{x}_k^-} - \psi \\ tan_2^{-1} \frac{y_{ref2,k} - \hat{y}_k^-}{x_{ref2,k} - \hat{x}_k^-} - \psi \end{bmatrix} \tag{2.24}$$

Where $(x_{ref1,k}, y_{ref1,k})$ are the coordinates of the first anchor

$$H_k = \frac{\partial h}{\partial \mathbf{x}}\bigg|_{\mathbf{x}=\hat{\mathbf{x}}_k^-} = \begin{bmatrix} \frac{\hat{x}_k^- - x_{ref1,k}}{d_{ref1,k}} & \frac{\hat{y}_k^- - y_{ref1,k}}{d_{ref1,k}} & 0 \\ \frac{\hat{x}_k^- - x_{ref2,k}}{d_{ref2,k}} & \frac{\hat{y}_k^- - y_{ref2,k}}{d_{ref2,k}} & 0 \\ \vdots & \vdots & \vdots \\ \frac{-(\hat{y}_k^- - y_{ref1,k})}{(d_{ref1,k})^2} & \frac{(\hat{x}_k^- - x_{ref1,k})}{(d_{ref1,k})^2} & -1 \\ \frac{-(\hat{y}_k^- - y_{ref2,k})}{(d_{ref2,k})^2} & \frac{(\hat{x}_k^- - x_{ref2,k})}{(d_{ref2,k})^2} & -1 \\ \vdots & \vdots & \vdots \end{bmatrix} \tag{2.25}$$

$$R_k = diag(\begin{bmatrix}\sigma^2_{dref1}, & \sigma^2_{dref2}, & \dots, & \sigma^2_{\alpha_1}, & \sigma^2_{\alpha_2}, & \dots\end{bmatrix}) \tag{2.26}$$

Where $d_{ref1,k} = \sqrt{(\hat{x}_k^- - x_{ref1,k})^2 + (\hat{y}_k^- - y_{ref1,k})^2}$.

Chapter 3

Simulation results

This chapter reports the results of the Matlab simulation of a localization system that uses the EKF to track a target moving on a certain trajectory at constant velocity. Ten anchors are assumed to be distributed in the space in fixed and known positions to perform the measurements. Three different simulations were executed using different State models and Measurements models of those discussed in the previous chapter: in the first simulation the filter uses the P model and acquires only distance measurements, in the second the filter uses the PV model and still collects only distance measurements, while in the third is simulated a hybrid ToA-AoA measurements model that estimates both the position and the orientation of the tag and uses the P model with the addition of the angle of rotation of the tag in the state vector as shown in 2.22. In Matlab, the shape of the trajectory of the tag is defined in a file .txt where for every segment of the tag path is declared the direction, the coordinates of the start and finish points and the speed of the target. From these data, the exact position of the tag is sampled at every time step $\Delta_T = 0.5s$ adding to the tag position the space traveled between two consecutive time steps at every cycle. The result is a vector with k sample of the exact tag position and knowing the position of the anchors, n distance measurements d_{MEAS} are computed for every sample, where n is the number of anchors that are in the proximity (<12m) of the tag and so can estimate correctly its position:

$$\begin{gathered} D_k(n) = \begin{bmatrix} x_{tag,k} \\ y_{tag,k} \end{bmatrix} - \begin{bmatrix} x_{anch,n} \\ y_{anch,n} \end{bmatrix} \\ d_{MEAS,k}(n) = \sqrt{D_k \cdot D_k^T} \end{gathered} \tag{3.1}$$

A random normally distributed noise with zero mean and standard deviation $\sigma_{d_{refk}} = 0.2m$ is added to the exact distance measurements d_{MEAS} to simulate the uncertainty of a real measurement. Finally, after obtaining the initial guess of the *a priori* estimate of the position following a linear least square approach [15], the

EKF is iteratively applied to the measurements step by step.

3.1 P Model with distance measurements

The first simulation takes just distance measurements and estimates the position of the tag. The State model and the measurement model used are those in equation (2.26)-(2.3) and in (2.14)-(2.17).

- **Parameters used for simulation**
  To simulate the Kalman Filter, certain parameters still need to be adjusted. The covariance $\mathbf{P}_0$ of the first *a priori* estimate was obtained by tuning the standard deviations for the two axes component of the position estimated (3.2). The process noise vector is modeled as a random velocity and so in order to compute its covariance as shown in (2.3) is needed to set the standard deviation σ_v of the random velocity (3.3). Lastly, the observation noise covariance $\mathbf{R}_k$ is obtained as a diagonal vector containing at each entry the variance $\sigma^2_{d_{refk}}$ of the ranging measurements. These choices lead to good results but real measurements should be considered to check if they fit well for the real scenario considered. The selection of the parameters is shown below:

$$\begin{gathered} P_0 = \begin{bmatrix} \sigma_x^2 & 0 \\ 0 & \sigma_y^2 \end{bmatrix}, \\ \sigma_x = \sigma_y = 0.3m \end{gathered} \tag{3.2}$$

$$\underbrace{\sigma_v = 2m/s}_{Q_k} \tag{3.3}$$

$$\underbrace{\sigma_{dref} = 0.2m}_{R_k} \tag{3.4}$$

- **Results**
  As each attempt produces slightly different outcomes due to measurement noise, the estimation of the tag location by the EKF is repeated ten times in order to evaluate the results. In the following figures, each sample is the mean of the results of ten trials. Every estimation has two components one on the x-axis and one on the y-axis, thus it is appropriate to evaluate the error and the RMSE on the singular axis:

$$\epsilon_x = \hat{x}_{tag,k} - x_{tag,k} \tag{3.5}$$

$$\epsilon_y = \hat{y}_{tag,k} - y_{tag,k} \tag{3.6}$$

$$RMSE_x = \sqrt{\mu^2_{\epsilon,x} + \sigma^2_{\epsilon,x}} \tag{3.7}$$

$$RMSE_y = \sqrt{\mu_{\epsilon,y}^2 + \sigma_{\epsilon,y}^2} \tag{3.8}$$

Where $(\hat{x}_{tag,k}, \hat{y}_{tag,k})$ is the position of the target estimated by the EKF, $(x_{tag,k}, y_{tag,k})$ is the exact position of the target, $\mu_{\epsilon,x}$ and $\sigma_{\epsilon,x}$ are the mean value and the standard deviation of ϵ_x while $\mu_{\epsilon,y}$ and $\sigma_{\epsilon,y}$ are the mean value and the standard deviation of ϵ_y.

Then the 2D localization error and its RMSE are computed as follows:

$$\epsilon = \sqrt{\epsilon_x^2 + \epsilon_y^2} \tag{3.9}$$

$$RMSE = \sqrt{\mu_\epsilon^2 + \sigma_\epsilon^2} \tag{3.10}$$

Where μ_ϵ is mean value of ϵ, and σ_ϵ^2 its variance.
For this configuration of the EKF, we get:
$\mu_{\epsilon,x} = -0.005m$, $\sigma_{\epsilon,x} = 0.153m$, $RMSE_x = 0.153m$,
$\mu_{\epsilon,y} = 0.000m$, $\sigma_{\epsilon,y} = 0.143m$, $RMSE_y = 0.143m$,
$\mu_\epsilon = 0.182m$, $\sigma_\epsilon = 0.104m$, $RMSE = 0.209m$.

Figure 3.1 reports in green the samples estimated by the EKF and how can be seen they track pretty well the trajectory. Figure 3.2 shows the average error on the axes and for every sample report the maximum, the minimum and the average error over 10 trials.

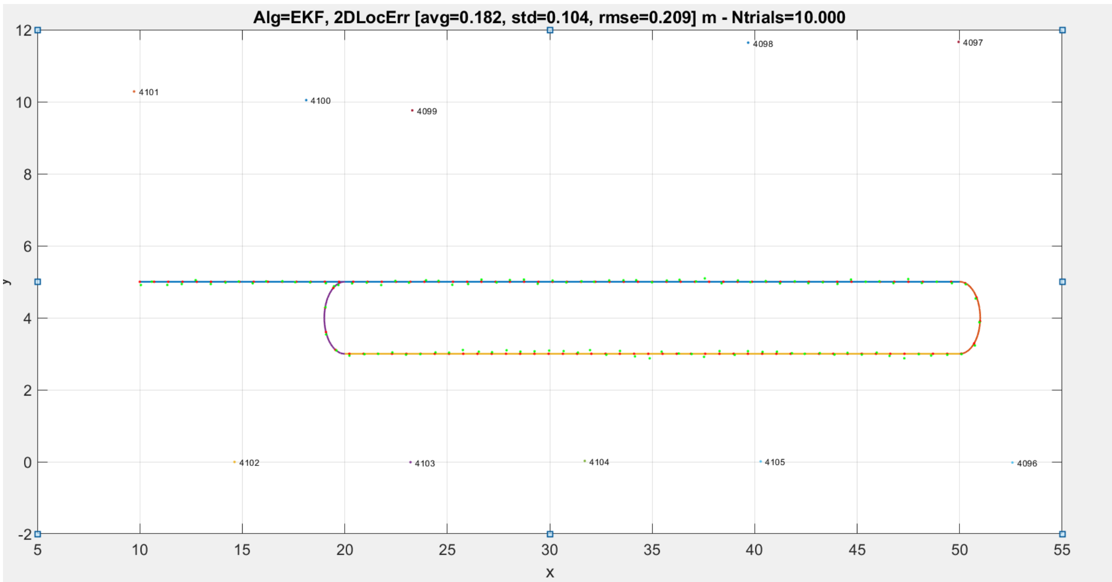

Figure 3.1: Tag trajectory (continuous line) and tag position sample estimated by the EKF (green dots)

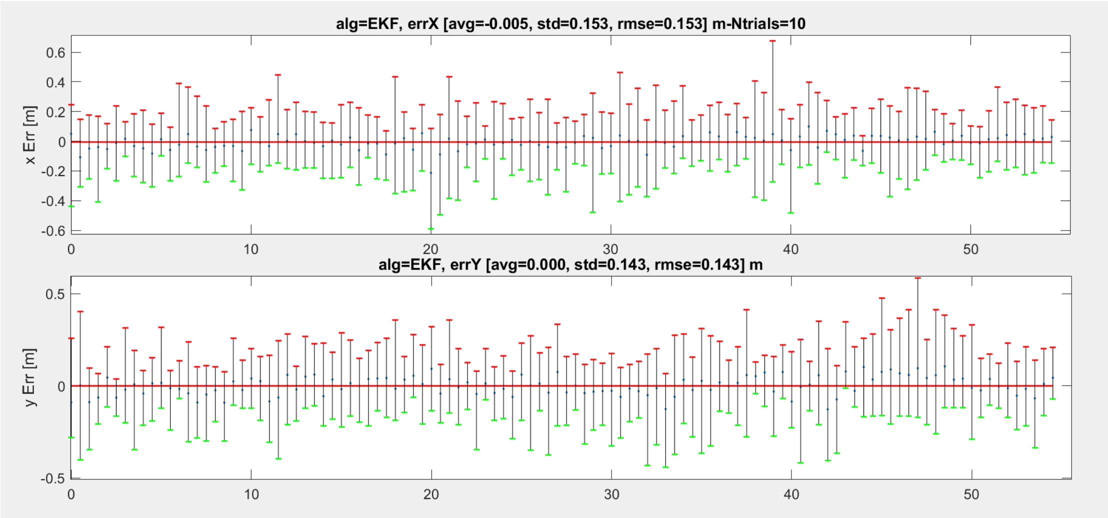

Figure 3.2: Average Measurement Error on the axes (red line), maximum, minimum and average error over 10 trials (red dashes, green dashes and blue dots)

3.2 PV Model with distance measurements

The second simulation is similar to the first one, but this time the speed of the tag is included in the state vector instead of considering only the position of the tag (P model). The State model and the measurement model used are those in equation (2.4)-(2.6) and in (2.14)-(2.17).

- **Parameters used for simulation** The parameters to be tuned are the same as the previous simulation but with the PV model the covariance P_0 of the *a priori* estimate contains obviously 4 columns, one for each state vector entry and the process noise vector this time is modeled as a random acceleration and not as a velocity. The selection of the parameters is shown below:

$$P_0 = \begin{bmatrix} \sigma_x^2 & 0 & 0 & 0 \\ 0 & \sigma_y^2 & 0 & 0 \\ 0 & 0 & \sigma_{v_x}^2 & 0 \\ 0 & 0 & 0 & \sigma_{v_y}^2 \end{bmatrix}, \sigma_x = \sigma_y = 0.3m, \sigma_{v_x} = \sigma_{v_y} = 0.1m/s$$

$$\underbrace{\sigma_a = 0.5m^2/s}_{Q_k}$$

$$\underbrace{\sigma_{dref} = 0.2m}_{R_k}$$

- **Results**
  In figures 3.3 and 3.4 are shown the results of this simulation. It can be seen that the trajectory is not tracked very well when the tag changes its direction of motion.

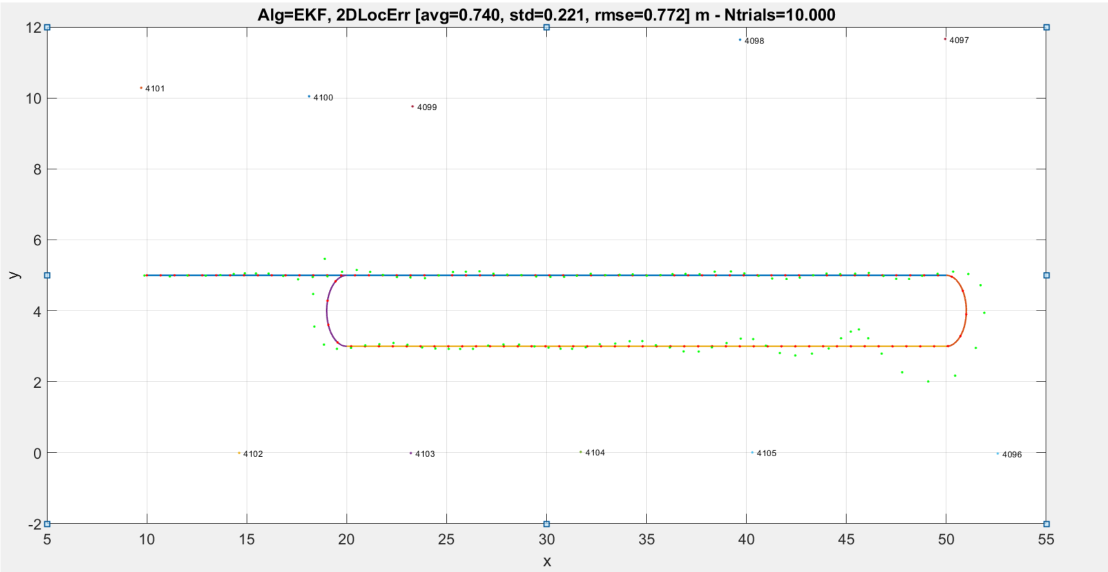

Figure 3.3: Tag trajectory (continuous line) and tag position sample estimated by the EKF (green dots)

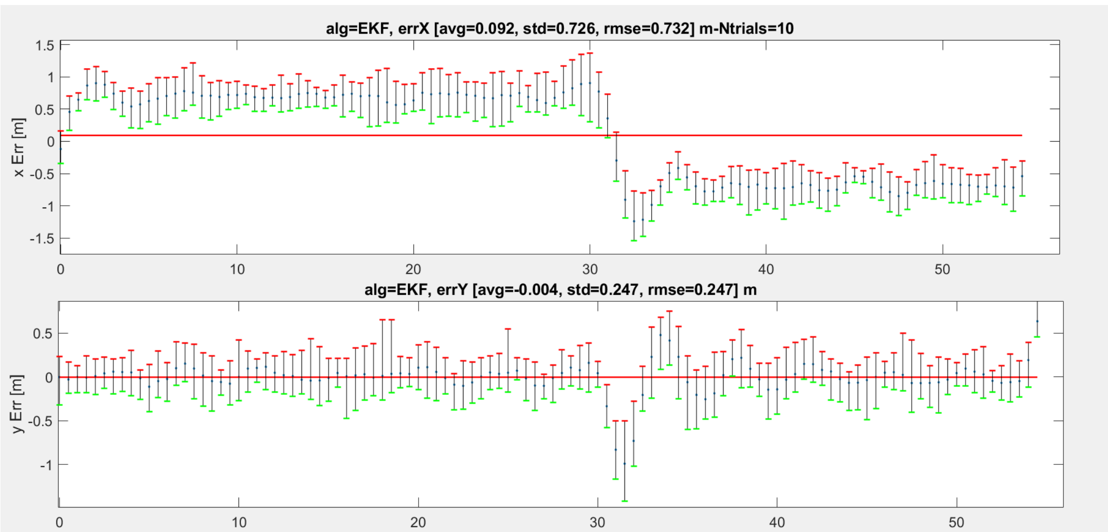

Figure 3.4: Average Measurement Error on the axes (red line), maximum, minimum and average error over 10 trials (red dashes, green dashes and blue dots)

For this configuration of the EKF, we get:
$\mu_{\epsilon,x} = 0.092m$, $\sigma_{\epsilon,x} = 0.726m$, $RMSE_x = 0.732m$,
$\mu_{\epsilon,y} = -0.004m$, $\sigma_{\epsilon,y} = 0.247m$, $RMSE_y = 0.247m$,
$\mu_{\epsilon} = 0.740m$, $\sigma_{\epsilon} = 0.221m$, $RMSE = 0.772m$.

3.3 Hybrid algorithm with both distance and AoA measurements

The last simulation estimate both the location and the orientation of the tag modifying the P model as shown in section 2.2.4.

- **Parameters used for simulation**
  The selection of the parameters is shown below:

$$P_0 = \begin{bmatrix} \sigma_x^2 & 0 & 0 \\ 0 & \sigma_y^2 & 0 \\ 0 & 0 & \sigma_\psi^2 \end{bmatrix}, \sigma_x = \sigma_y = 0.3m, \sigma_\psi = 2^\circ$$

$$\underbrace{\sigma_v = 1m/s, \sigma_\omega = 40^\circ/s}_{Q_k}$$

$$\underbrace{\sigma_{dref} = 0.2m, \sigma_{\alpha_1} = 5^\circ}_{R_k}$$

- **Results** For this configuration of the EKF, we get:
  $\mu_{\epsilon,x} = -0.010m$, $\sigma_{\epsilon,x} = 0.150m$, $RMSE_x = 0.151m$,
  $\mu_{\epsilon,y} = 0.011m$, $\sigma_{\epsilon,y} = 0.130m$, $RMSE_y = 0.131m$,
  $\mu_{\epsilon,\theta} = -0.037^\circ$, $\sigma_{\epsilon,\theta} = 2.420^\circ$, $RMSE_\theta = 2.420^\circ$,
  $\mu_{\epsilon} = 0.174m$, $\sigma_{\epsilon} = 0.097m$, $RMSE = 0.199m$.

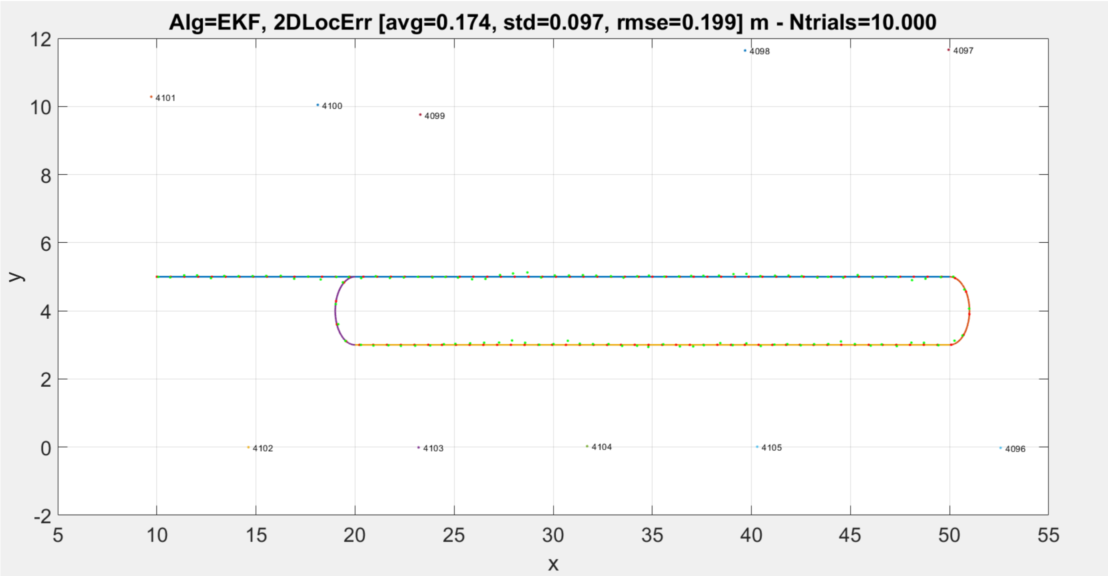

Figure 3.5: Average Measurement Error on the axes (red line), maximum, minimum and average error over 10 trials (red dashes, green dashes and blue dots)

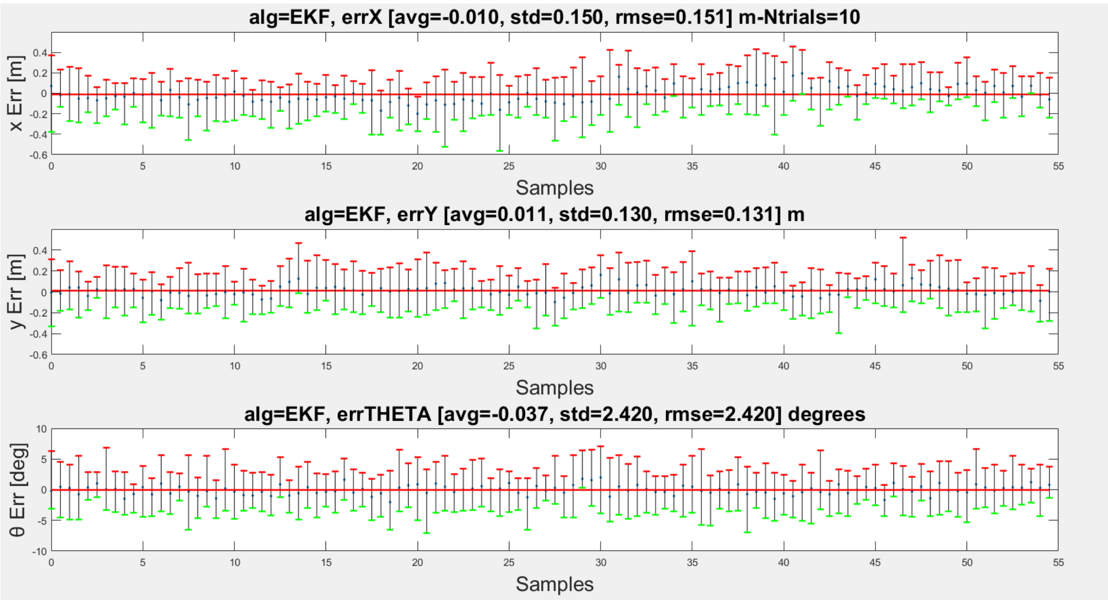

Figure 3.6: Average Measurement Error on the axes (red line) and on the estimation of the orientation θ, maximum, minimum and average error over 10 trials (red dashs,green dashs and blue dots)

3.4 Discussion

The results show significantly better results for the hybrid configuration. This configuration offers good accuracy in the estimation of the orientation, in fact, $\sigma_{\epsilon,\theta} = 2.429°$ starting from a standard deviation on the AoA measurements $\sigma_{\alpha_1} = 5°$. Also the estimation of the tag position is very accurate and better than the other two configurations because considering more measurements, also of different types, the EKF predicts better the tag. Instead, the simulation that gives the worst results is the second where the accuracy collapses when the tag changes its direction. Even worse results would have been obtained if the speed of the tag had not been completely constant because the filter corrects the position estimation on the basis of the velocity but it does not measure it.

Chapter 4

Real PDoA-ToA Measurements using 3 antennas

In this chapter a possible setup to acquire real ToA and AoA measurements will be discussed and then the measurement error will be analyzed.
In fact, while in the previous chapters the measurements were derived starting from the exact estimation and adding an additive White Gaussian Noise (AWGN) with known variance, in this section a UWB kit produced by Mobile Knowledge was used to take the measurements. It includes a battery-powered tag and an anchor with an antenna array placed on it that allows to estimate the AoA (α), in addition to the ToA and the RSSI, deriving it from PDoA measurements as seen in section 1.1.4. Substituting all the terms, we get:

$$\alpha = \arcsin \frac{PDoA \cdot c}{2\pi \cdot A_{dist} \cdot f} \tag{4.1}$$

Where:
$c = 299792458 m/s$ is the speed of light,
$A_{dist} = 0.0187 m$ is the distance between the antennas of the anchor,
$f = 6489600000 Hz$ is the frequency of the signal.
To evaluate the measurement error, the measurements estimated by the UWB kit will be compared with those of VICON, a very accurate Infra Red camera-based localization system installed in the lab.

4.1 Anchor Calibration

Although the equation in 4.1 provides the AoA, this is an indicative estimate that in many cases does not accurately represent the true relationship between AoA and PDoA which is different for every anchor. For this reason, is needed a calibration for each anchor used. The idea is to place the anchor with a known orientation, collect the corresponding PDoA measurement, and then repeat with different angles to obtain a lookup table. To do this, With the aid of a robotic hand in the lab the anchor was rotated about the vertical axis between $-85°$ and $+85°$ changing the orientation of the anchor every 30 seconds, while the tag was placed on a tripod at the same height as the anchor (1.52m) at a horizontal distance of 2.66m. Since the measurements are less accurate in the extremes of this range, for $\alpha < -60°$ and $\alpha > +60°$ the anchor rotates by $5°$ every time step in order to collect more samples, while for $-60° < \alpha < +60°$ the anchor rotates by $10°$. In figure 4.1 can be seen the PDoA measured for the 23 orientations considered.

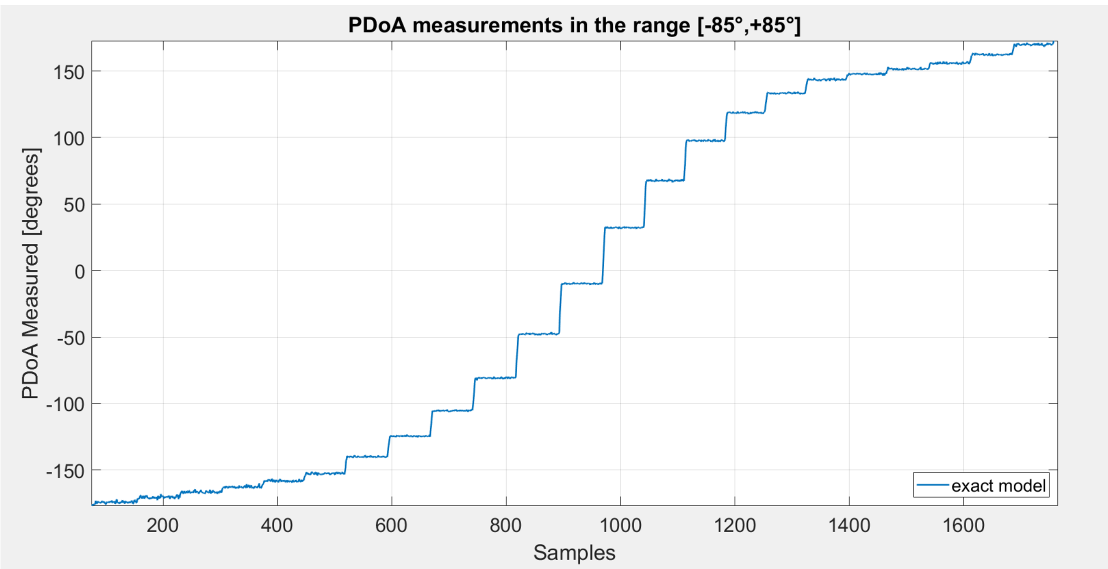

Figure 4.1: PDoA measurements in the range [-85°,+85°]

Then, a LUT as the one in figure 4.2 can be constructed, where the items in the first column are the mean values of the PDoA measured at each of the 23 orientations of the anchor, while those in the second column are the corresponding expected PDoA values calculated with the formula in 4.3.
The data points in the LUT are then linearly interpolated finding the lines passing through each pair of consecutive points of the LUT to obtain a piecewise linear function that corrects the PDoA measurements.

```
lutPdoA = [
        % PDoAMeas          PDoACorrected
          -173.3668         -145.6930           % +85°
          -168.9054         -144.0277           % +80°
          -164.3331         -141.2662           % +75°
              ⋮                 ⋮
          -76.3651          -50.0203            % +20°
          -43.0878          -25.3960            % +10°
          -4.8756           0                   %   0°
          36.7268           25.3960             % -10°
          72.1329           50.0203             % -20°
              ⋮                 ⋮
          159.6595          141.2662            % -75°
          164.6476          144.0277            % -80°
          170.0315          145.6930 ];         % -85°
```

Figure 4.2: PDoA LUT

4.2 Compensate the difference in height between the tag and the anchor

The measured distance d_{MEAS} is the length of the direct path that connects the tag and the anchor, and so if the tag and the anchor are placed at different heights it does not correspond to the projection of the distance on the x-axis. Since we are interested in a 2D localization of the target on the floor some geometrical corrections must be included as shown in figure 4.3. The corrected distance d_{CORR}

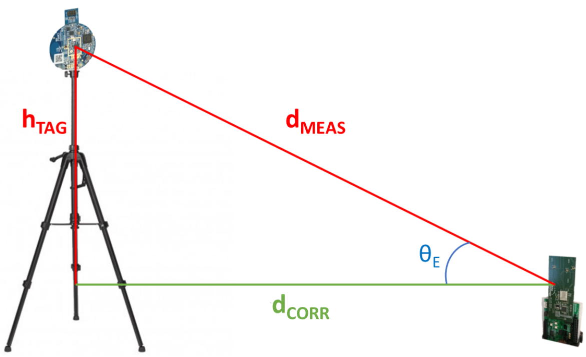

Figure 4.3: Distance corrections

can be simply calculated applying the Pythagorean theorem.

$$d_{CORR} = \sqrt{d_{MEAS}^2 - h_{TAG}^2} \tag{4.2}$$

For the same reason, also the AoA measurements need to be projected on the x-axis. In fact, in figure 4.4 it can be seen that the AoA α is measured on the plane where lies d_{MEAS}. After some geometrical consideration, is possible to obtain the formula in 4.3 to correct α.

$$\alpha_{CORR} = \arcsin \frac{d_{CORR}}{d_{MEAS} \cdot \sin \alpha} \tag{4.3}$$

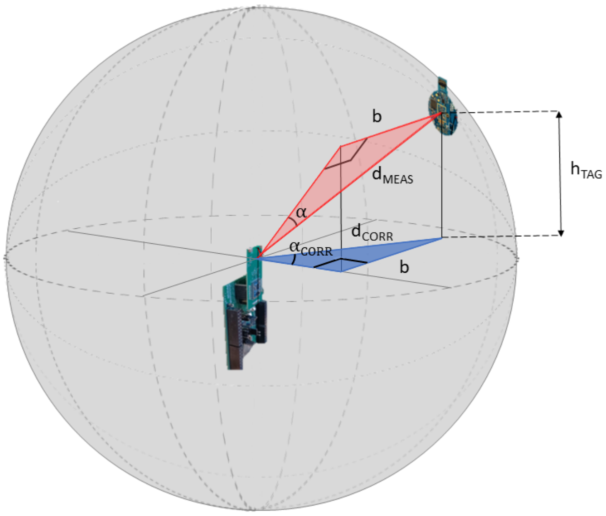

Figure 4.4: AoA corrections

4.3 Measurements feasibility at different elevation angles

At this point, it is important to understand if the calibration of the anchor and the projection correction are sufficient to guarantee an accurate estimation for any difference in height between the tag and the anchor or better, for any elevation angle θ_E defined as shown in figure 4.3.
The results in figure 4.5 show that increasing the elevation angle, the accuracy of the estimation gets worse until in the extremes of the range the PDoA saturates. This means that in the extremes, the same PDoA value corresponds to different orientations making them indistinguishable and so reducing the range in which the estimation made by the anchor is reliable. The simulations show that the elevation angle must not exceed 20° to guarantee a reliable range of $[-60°, +60°]$.

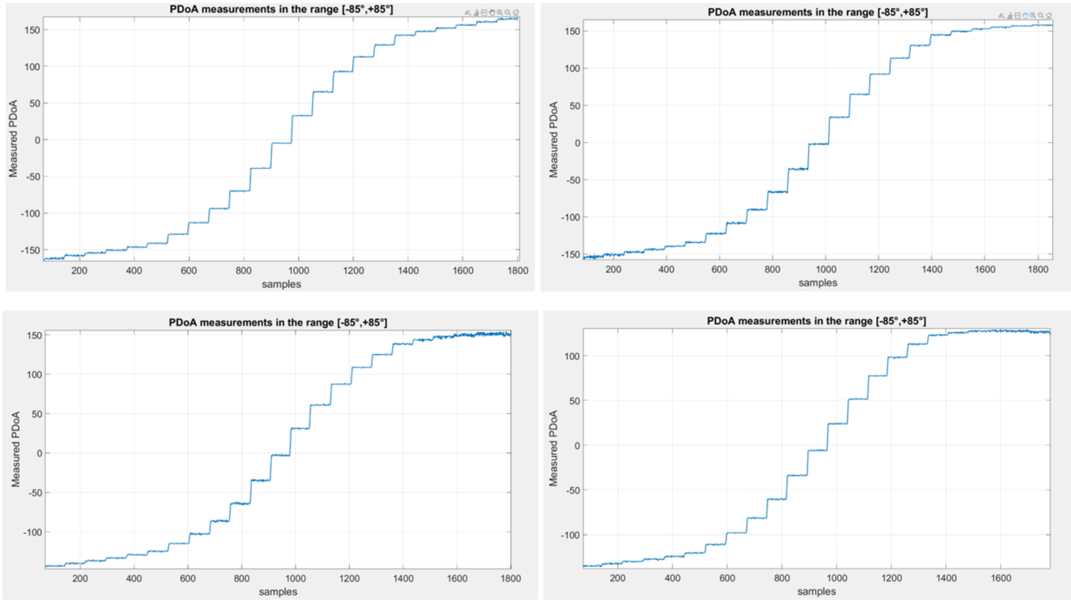

Figure 4.5: PDOA measurements in the range [-85°,+85°] with an elevation angle equals to 16° (top left), 21° (top right),26° (bottom left), 34° (bottom right)

4.4 360° measurements coverage

A single anchor at the same height as the tag can accurately perform measurements in the range $[-82°, +82°]$, and as seen in the previous paragraph this range decreases as the elevation angle increases. Thus, more than one anchor must be integrated to allow a 360° localization of a certain target. Assuming that the elevation angle does not exceed 20°, a single antenna can cover a range of 120° where it can reliably measure the AoA and so three anchors are required for 360° coverage. In figure 4.6 is shown a possible configuration of the three anchors.

Depending on the orientation of the three anchors with respect to the tag, the anchor that is best directed toward the tag will produce the measurement. In the limit case shown in figure 4.7, two anchors can perform the measurement because they are both rotated by 60° with respect to the tag, so is possible to combine the two observations via data fusion.

4.5 RSSI measurements

To find the anchor that effectively is most pointed towards the tag, the RSSI measurements produced by the anchors can be used. In fact, an anchor with its front side directed toward the tag will receive a stronger signal with respect to

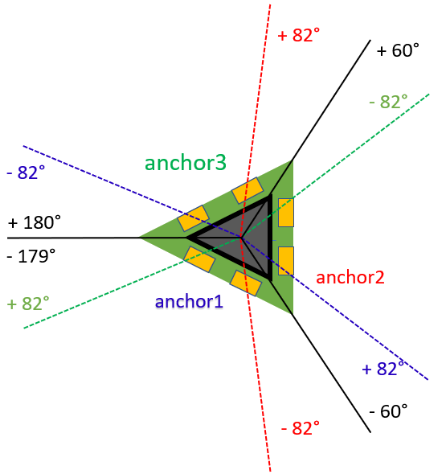

Figure 4.6: Anchors configuration to allow 360° coverage.

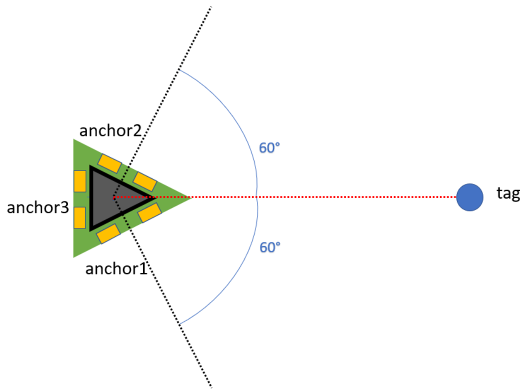

Figure 4.7: Limit case suitable for data fusion

an anchor reached by the signal from behind. For any configuration, finding the maximum RSSI among those measured, it is possible to select the anchor that must produce the AoA measurements. To take these measurements in the lab, a radio-absorbent paper was placed on the back of the anchors to maximize the difference between the RSSI received by the antenna in front of the tag and the other and then, the three antennas were placed on a Turtlebot3 connected to the integrated Raspberry Pi which ran a firmware that sequentially collects the measurements of the anchors. The tag, placed on a tripod at a known height, was moved each time to test different configurations of the system. The cage in which the anchors were tested is equipped with VICON, a very accurate camera-based tracking system that can individuate the Turtlebot recognizing a certain number of markers uniquely arranged on it and estimate its position and orientation with an accuracy of about 0.1°. The VICON measurements can be considered as a ground truth to calculate the accuracy of the localization via UWB. In figure 4.8 it can be seen the setup of the instrumentation in the lab and the arrangement of anchors and markers on the Turtlebot, while in figure 4.9 is reported a screenshot of the software interface of the VICON system.

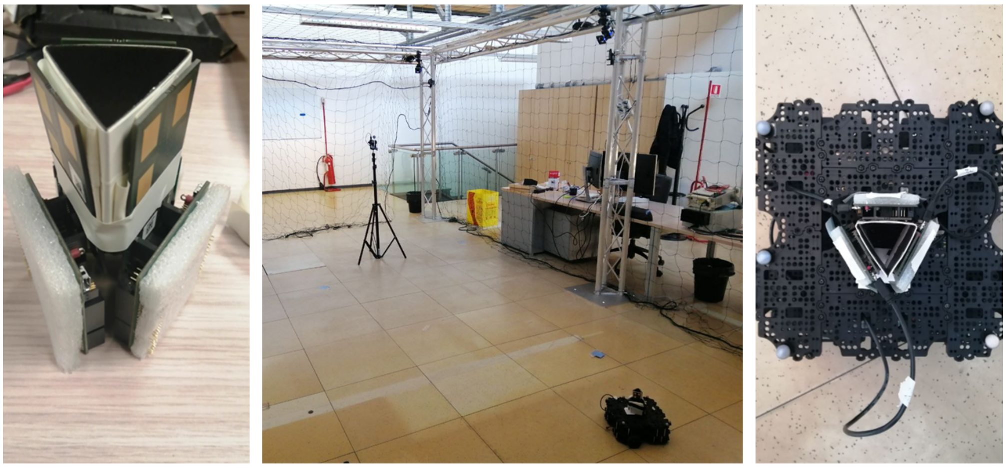

Figure 4.8: On the left the three anchors shifted of 120°, in the center is possible to see the VICON cameras in the corners of the cage and on the right the TurtleBot with the anchors and the marker placed on.

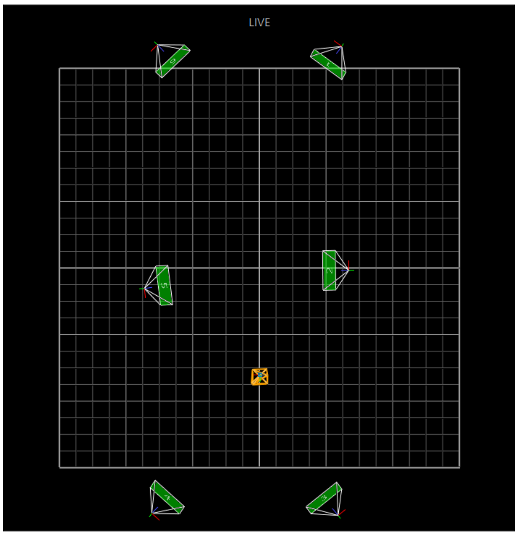

Figure 4.9: Screenshot of the software interface of VICON. It can be seen the arrangement of the cameras and the Turtlebot3

Four static orientations of the TurtleBot3 (shown in figure 4.10) were considered to evaluate the difference in RSSI between the anchors. The measurements were collected for one minute to have different samples for every static configuration. The results are shown in figure 4.11, where on the x-axis are reported the angles of rotation expressed in degrees corresponding to the four orientations of the TurtleBot3 shown in figure 4.10 and on the y-axis the RSSI values obtained from the three antennas. It can be seen that in the first configuration, anchor 2 is perfectly aligned with the tag while anchor 1 and anchor 3 are both directed with their back to the tag with an angle of rotation of 120°, in fact in the graph it is possible to see that the RSSI measured by anchor 2 is the highest, while the other two anchors measure a similar and much lower RSSI because they are rotated by the same angle with respect to the tag. Passing from one configuration to another, the RSSI measured by anchor 1 increases as it becomes more oriented toward the tag. In the third configuration, the limit case discussed before in which two anchors are oriented in such a way that they can both carry out the measurement occurs. Anchor 1 and anchor 2 have a similar RSSI, therefore it is not possible to select one of them just on the basis of the RSSI. However, both of them can carry out the measurements and so the choice can be made arbitrarily or a data fusion strategy can be considered.

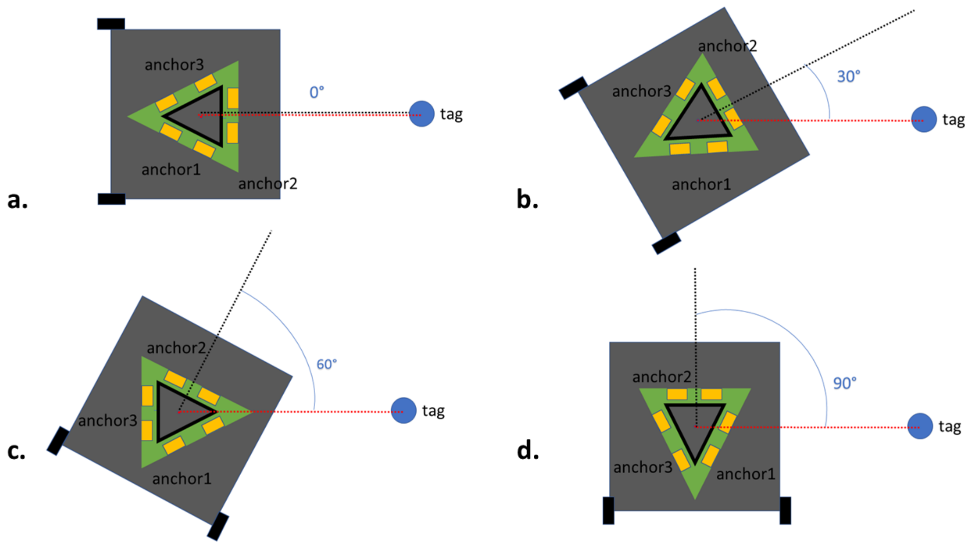

Figure 4.10: 4 orientation of the TurtleBot3

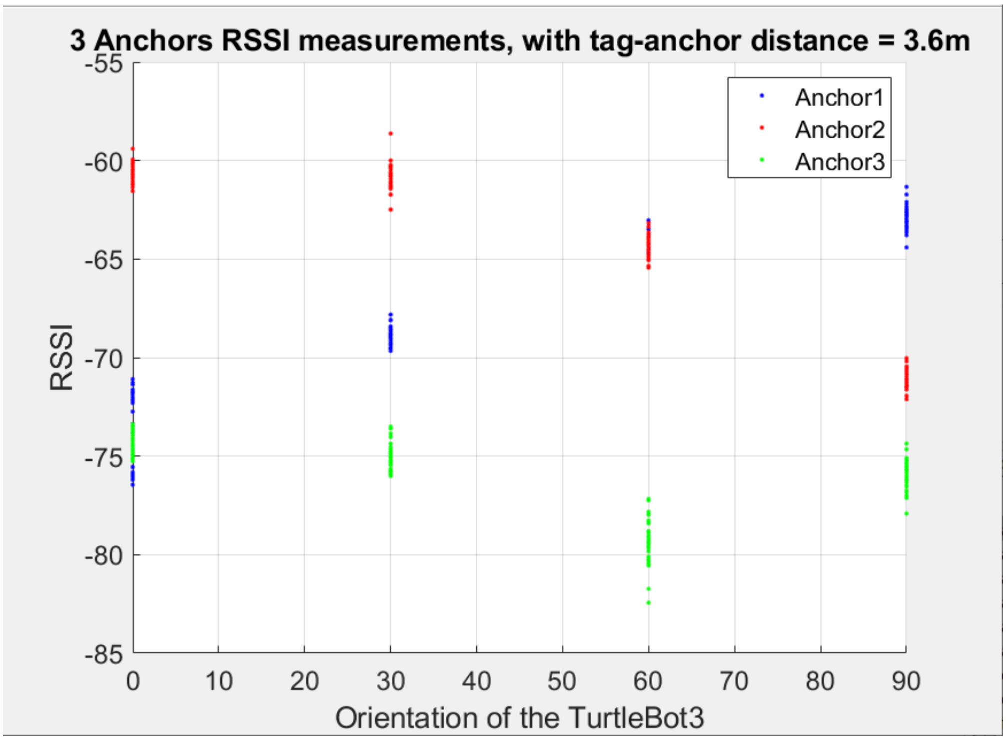

Figure 4.11: 3 Anchors RSSI measurements, with tag-anchor distance = 3.6m and elevation angle $\theta_E = 16°$

4.6 Static Measurements

Lastly, the accuracy of the ToA and AoA estimates produced by the UWB kit was evaluated through several static measurements. In fact, it was not possible to carry out real-time measurements of a moving object because the firmware collects the measurements of the three anchors sequentially and was not able to achieve a delay of less than 500 ms between the collection of the measurements of two consecutive anchors. As was already stated, it is necessary to have access to all three antennas' RSSI measurements since only the data generated by the anchor with the highest RSSI value are picked. Thus, if the localization target moves when the algorithm is still waiting to collect all the measures, it makes no sense to compare the RSSI of the three anchors because they are referred to different locations and orientations of the target. In static conditions, the accuracy of the measurements depends on different factors. First of all, the measurement accuracy decreases as the angle of rotation of the anchor with respect to the tag increases, if the anchor is directed exactly toward the tag the measurements will be significantly more accurate. Regarding the AoA measurements, the elevation angle has an impact on the accuracy of AoA measurements since, above 20°, the calibration of PDoA measurements performed with the tag and anchor at the same height is no longer valid. Furthermore, since the ToA measurements are utilized to adjust the AoA measurements to account for the height difference between the tag and the anchor using the calculation in 4.3, the accuracy of AoA measurements is highly dependent on the accuracy of ToA measurements. The ToA and AoA measurements were evaluated as done before for the RSSI measurements, connecting the anchors to the TurtleBot3, collecting several samples for each of the four static orientations shown in figure 4.10 and selecting the anchor with the highest RSSI. Looking at the graph shown in figure 4.11 it can be seen that, for every orientation of the TurtleBot3, the anchor with the greatest RSSI is always the one that is more directed toward the tag, and there is no overlap between the samples produced by the anchor with the highest RSSI and the others. Nonetheless, it is possible that overlap will arise if the tag-anchor distance is decreased or the elevation angle is changed. It's crucial to prevent this as it indicates that for some configurations the anchor that should be chosen does not have the highest RSSI. Figures 4.12 and 4.13 show the ToA and AoA estimation errors achieved in each of the four TurtleBot orientations taken into account, as well as at various distances from the tag. For each anchor in each configuration, only one sample was taken into account, and only the measurements recorded by the anchor with the highest RSSI were shown.

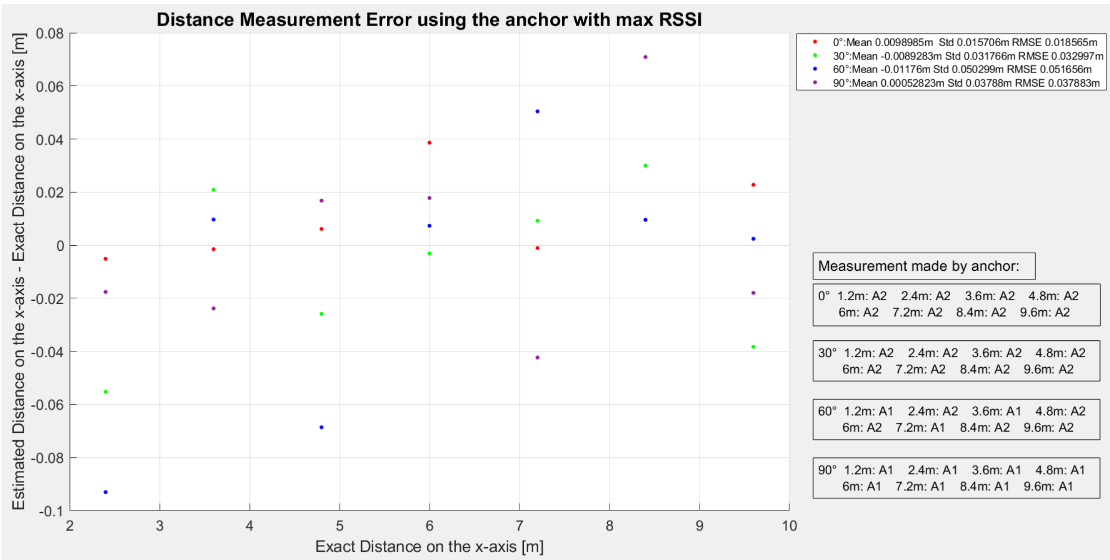

Figure 4.12: ToA measurement error

In the figures on the x-axis is reported the exact tag-anchors distance while on the y-axis the measurement error. The samples corresponding to the different orientations of the TurtleBot3 are overlaid and indicated with different colors.

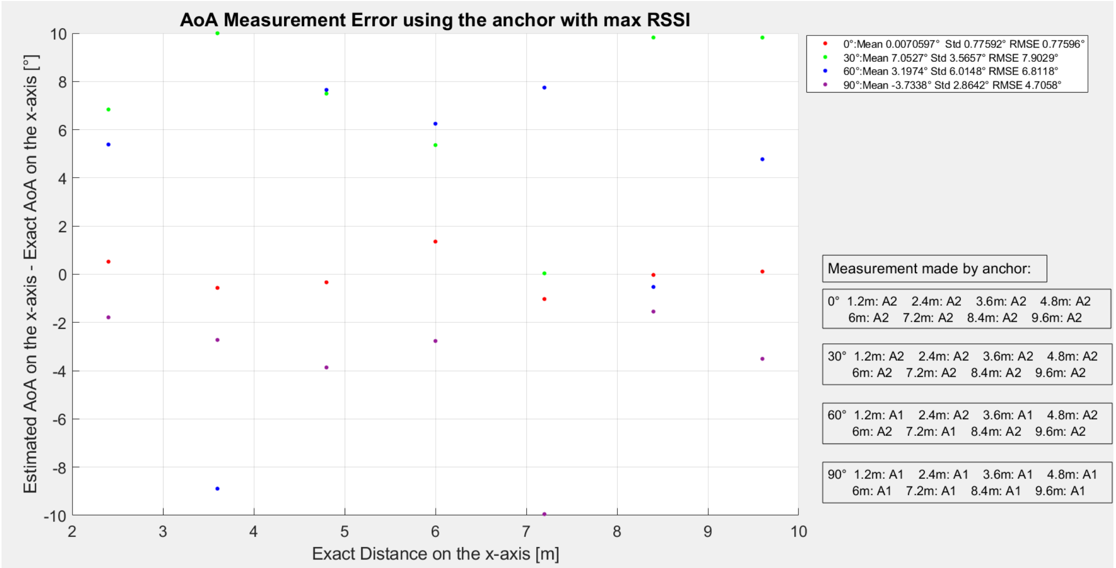

Figure 4.13: AoA measurement error

At the bottom right of the figures are printed the anchors selected to collect the measurements for each configuration and it is possible to see that is always chosen the proper anchor. In the limit case when the TurtleBot is rotated by 60°, the algorithm sometimes chooses anchor 1 and other times anchor2 since both have a high and comparable RSSI, and this is the configuration for which data fusion could be applied, even because correspond to the configuration with the least accurate measurements. The distance estimation seems to be quite accurate ensuring an error of about $\pm 0.1m$ for every configuration after adding a bias computed across all the samples and not only the ones plotted in the figures. The mean, the standard deviation of the ToA measurement error and the Root-Mean-Square Error (RMSE) calculated for the sample in the graph are reported in the following:

0°:Mean 0.0098985m Std 0.015706m RMSE 0.018565m,
30°:Mean -0.0089283m Std 0.031766m RMSE 0.032997m,
60°:Mean -0.01176m Std 0.050299m RMSE 0.051656m,
90°:Mean 0.00052823m Std 0.03788m RMSE 0.037883m.

The AoA measurements, instead, are less accurate with an error of about ±10°. This is due to the fact that most of the configurations under study were made at high elevation angles, as well as the fact that the projection correction propagates the distance error to the AoA. The mean, the standard deviation of the AoA measurement error and the Root-Mean-Square Error (RMSE) are reported in the following:

0°:Mean 0.0070597° Std 0.77592° RMSE 0.77596°,
30°:Mean 7.0527° Std 3.5657° RMSE 7.9029°,
60°:Mean 3.1974° Std 6.0148° RMSE 6.8118°,
90°:Mean -3.7338° Std 2.8642° RMSE 4.7058°.

Analyzing the graphs and the RMSE values obtained for the AoA measurements, it can be seen that the error increases as the rotation angle of the TurtleBot3 with respect to the tag increases.

Chapter 5

Conclusion

The aim of this thesis was to design different real-time localization solutions for indoor environments based on UWB technology that enable autonomous navigation. Three distinct designs that varied for the building of the state and the measurement model were used to simulate an EKF in Matlab that combined the UWB measurements. It was discovered that the hybrid approach that included both ToA and AoA measurements had the best results in terms of estimation errors.
Then, in order to evaluate real measurement errors, real PDoA and ToA measurements were obtained in the lab using a UWB kit for different static positions and orientations of the anchors to evaluate real measurement errors. In fact, the firmware that manages the anchors is not able to collect the data fast enough to permit the target to move during the measurements. For this reason and for the lack of availability of more than one tag it was not possible to simulate the EKF with the real measurements acquired in the lab. When the measurement errors were examined, it was found that the ToA measurement had a fairly high degree of accuracy while the AoA measurements had a lower degree of accuracy for various reasons related to the placement of the antennas with respect to the tag and the propagation of noise during the correction of the AoA measurements to account for the height difference between the tag and the anchors. The RSSI-based selection of the anchor was tested in a variety of tag and anchor positions, and it consistently produced positive results.

5.1 Further Work

In order to implement the hybrid algorithm based on the EKF is necessary to acquire the measurements of the three anchors simultaneously for every time step. A solution could be the implementation of a Time Division Multiple Access (TDMA) based protocol, in fact, interferences are prevented using a scheduling algorithm,

therefore is not necessarily essential to acquire the measurements sequentially and with a high latency.
A further step to improve the performances of the EKF it can be to use also IMU measurements in addition to the UWB measurements used so far. In fact, IMU measurements are typically acquired at a higher rate than UWB measurements, but their accuracy degrades rapidly over time compared to more precise UWB measurements. Therefore, it is feasible to combine the benefits of both the measurement models and lessen their drawbacks by using both IMU and UWB measurements in the EKF.

Appendix A

The Extended Kalman Filter

The Kalman Filter is an efficient solution to the least-squares estimator problem introduced by R.E. Kalman in 1960. It estimates recursively the state of a process solving the minimum least-squares error problem for applications that can be represented as a linear system driven and disturbed by Gaussian noise. The Kalman Filter work for process that can be modeled as a linear system affected by Gaussian distributed noise. However, if the process to be estimated or the measurement relationship to the process is non-linear the Kalman Filter can be extended with some linearizations and approximations to his version suitable for non-linear systems, referred as Extended Kalman Filter (EKF). The discrete EKF estimates recursively the state of a dynamic system modeled by a discrete-time state equation:

$$\begin{aligned} \mathbf{x}_k &= f(\mathbf{x}_{k-1}) + \mathbf{w}_k, \\ p(\mathbf{w}_k) &\sim \mathcal{N}(0, \mathbf{Q}_k), \end{aligned} \tag{A.1}$$

Where $\mathbf{x}_k$ is the *state vector* at time k, f is the *state transition function* that propagates the state in time given the previous state $\mathbf{x}_{k-1}$. The *process noise vector*$\mathbf{w}_k$ takes into account the unknown deviations from the system model, assumed to be a vector of random noise normally distributed with zero mean and covariance matrix $\mathbf{Q}_k$.
The system is observed through the measurement equation:

$$\begin{aligned} \mathbf{z}_k &= h(\mathbf{x}_{k-1}) + \mathbf{v}_k, \\ p(\mathbf{v}_k) &\sim \mathcal{N}(0, \mathbf{R}_k), \end{aligned} \tag{A.2}$$

Where $\mathbf{z}_k$ is the *measurement vector* at time k, h is the *observation function* that estimates the expected measurements at the true state $\mathbf{x}_k$ and $\mathbf{v}_k$ is the *observation noise vector* modeled by a vector of random noise normally distributed with zero mean and covariance matrix $\mathbf{R}_k$.

The EKF iteratively tracks the state evolution of the system in two phases by using a form of feedback control: the *predict phase* propagates the state and the error covariance in time to obtain the *a priori* estimates, while the *update phase* is responsible for the feedback because correct the *a priori* estimate integrating a new measurement to obtain an improved *a posteriori* estimate.

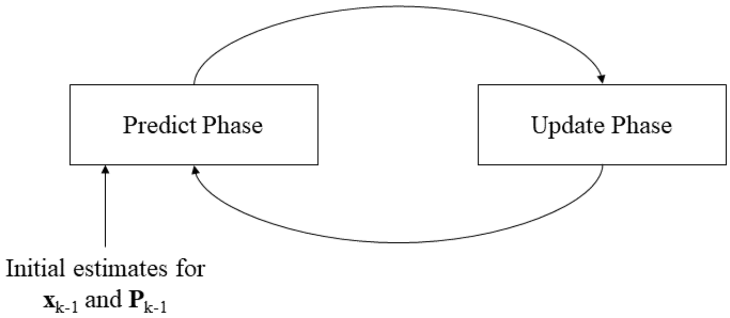

Figure A.1: The discrete Kalman Filter cycle

A.1 Predict Phase

In this phase the *a priori* state vector estimation $\hat{\mathbf{x}}_k^-$ and its covariance $\hat{\mathbf{P}}_k^-$ are computed at time k on the basis of the previous *a posteriori* state estimate $\hat{\mathbf{x}}_{k-1}^+$ at time *k-1*, its covariance $\hat{\mathbf{P}}_{k-1}$ and the process noise covariance matrix $\mathbf{Q}_k$:

$$\hat{\mathbf{x}}_k^- = f(\hat{\mathbf{x}}_{k-1}^+, \hat{\mathbf{u}}_{k-1}) \tag{A.3}$$

$$\hat{\mathbf{P}}_k^- = \mathbf{F}_k \hat{\mathbf{P}}_{k-1}^+ \mathbf{F}_k^T + \mathbf{Q}_k \tag{A.4}$$

Where $\mathbf{F}_k = \frac{\partial f}{\partial \mathbf{x}}\Big|_{\mathbf{x}=\hat{\mathbf{x}}_k^-}$ is the Jacobian matrix of the state transition function f computed around the previous estimates.

A.2 Update Phase

First of all, in this phase when a new measurement $\mathbf{z}_k$ become available the *innovation vector* $\mathbf{y}_k$ is calculated as the residual between the observed measurement $\mathbf{z}_k$ and the expected measurement $h(\hat{\mathbf{x}}_k^-)$, while its covariance matrix $\mathbf{S}_k$ as the expected measurement estimation error due to the *a priori* state error covariance plus the measurement covariance $\mathbf{R}_k$:

$$\mathbf{y}_k = \mathbf{z}_k - h(\hat{\mathbf{x}}_k^-) \tag{A.5}$$

$$\mathbf{S}_k = \mathbf{H}_k \hat{\mathbf{P}}_k^- \mathbf{H}_k^T + \mathbf{R}_k \tag{A.6}$$

Where $\mathbf{H}_k = \frac{\partial h}{\partial \mathbf{x}}\Big|_{\mathbf{x}=\hat{\mathbf{x}}_k^-}$ is the Jacobian matrix of the observation function h computed around the previous estimates. Then, the filter computes the *a posteriori* state vector estimate $\hat{\mathbf{x}}_k^+$ and its covariance $\hat{\mathbf{P}}_k^+$, correcting the *a priori* estimates $\hat{\mathbf{x}}_k^-$ and $\hat{\mathbf{P}}_k^-$:

$$\hat{\mathbf{x}}_k^+ = \hat{\mathbf{x}}_k^- + \mathbf{K}_k \mathbf{y}_k \tag{A.7}$$

$$\hat{\mathbf{P}}_k^+ = (I - \mathbf{K}_k \mathbf{H}_k) \hat{\mathbf{P}}_k^- \tag{A.8}$$

Where $\mathbf{K}_k$ is the optimal *Kalman Gain* :

$$K_k = \hat{P}_k^- H_k^T S_k^{-1} \tag{A.9}$$

Appendix B

Coordinate systems

Various coordinate systems have been used in target tracking, such as Earth-Centered Earth-Fixed Frame (ECEF), Inertial Frame (i-frame), Local Geodetic Frame (t-frame) and Body Frame (b-frame). In this section is presented a brief overview of the most used ones.

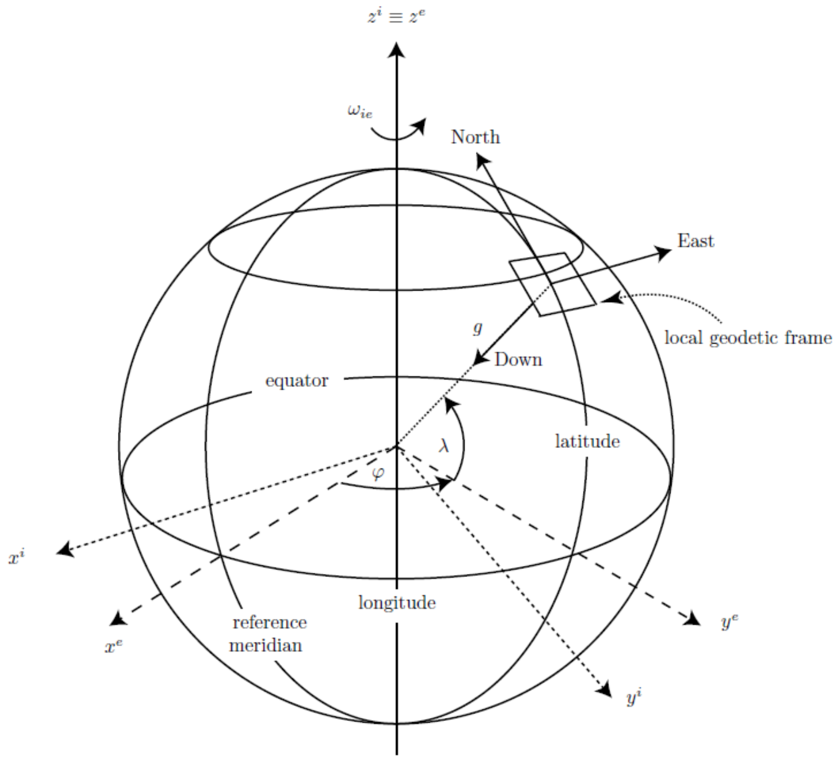

Figure B.1: ECEF (e-frame), local geodetic (t-frame), and inertial (i-frame) frame relationships.

B.1 Earth-Centered Earth-Fixed Frame (ECEF)

The ECEF coordinate system, also referred to as geocentric coordinate system is a Cartesian spatial reference system that represents locations close to the Earth. It has its origin at the center of mass of the Earth and rotate with the Earth. The axes are directed as follows: the x-axis points towards the intersection between the prime meridian and the equator, the z-axis is the line between the North and South Poles, with positive values increasing northward and the y-axis is in the plane of the equator and complete the right-handed coordinate system.

B.2 Inertial Frame

An inertial frame is a coordinate system that can be in linear motion but is not accelerating and so Newton's laws of motion can be applied. The origin of the system and the directions of the axes are arbitrary as long as the right-hand rule is respected. Usually, it is preferable to consider the origin in the center of mass of Earth, the z-axis pointing toward the North Pole, the x-axis and y-axis lying on the equator plane. In this way, this coordinate frame is consistent with the ECEF and differs from it only because does not rotate with the Earth.

B.3 Local Geodetic Frame (NED, ENU)

This coordinate system has its origin in a fixed point of the Earth surface, the z-axis point towards the earth's interior (down), the x-axis and the y-axis lie on a plane tangent to the origin and point toward the local North direction and the local South direction. This coordinate configuration is referred to as North-East-Down (NED), but another right-handed variant exists and is called East-North-Up (ENU).

B.4 Body Frame

The Body Frame is the coordinate system attached to the vehicle. Its origin is at the center of gravity of the vehicle, the x-axis points in the forward direction, the z-axis down through the vehicle and the y-axis completes the right-hand coordinate system.

B.5 Platform Frame

The Platform Frame is the coordinate system of the platform where the sensors that acquire measurements are mounted on. This frame is needed in applications where the platform is not aligned with the body frame and so the two coordinate system are not coincident.

Bibliography

[1] Faheem Zafari, Athanasios Gkelias, and Kin K. Leung. «A Survey of Indoor Localization Systems and Technologies». In: *IEEE Communications Surveys & Tutorials* 21.3 (2019), pp. 2568–2599. DOI: 10.1109/COMST.2019.2911558 (cit. on pp. 1, 7, 8).

[2] Christos Laoudias, Adriano Moreira, Sunwoo Kim, Sangwoo Lee, Lauri Wirola, and Carlo Fischione. «A Survey of Enabling Technologies for Network Localization, Tracking, and Navigation». In: *IEEE Communications Surveys & Tutorials* 20.4 (2018), pp. 3607–3644. DOI: 10.1109/COMST.2018.2855063 (cit. on p. 1).

[3] Dr. Brian Gaffney. «A survey of indoor positioning systems for wireless personal networks». In: *IEEE Communications Surveys & Tutorials* 11.1 (2009), pp. 13–32. DOI: 10.1109/SURV.2009.090103 (cit. on pp. 1, 2).

[4] Roy Want, Andy Hopper, Veronica Falcão, and Jonathan Gibbons. «The Active Badge Location System». In: *ACM Trans. Inf. Syst.* 10.1 (Jan. 1992), pp. 91–102. ISSN: 1046-8188. DOI: 10.1145/128756.128759. URL: https://doi.org/10.1145/128756.128759 (cit. on p. 5).

[5] E. Aitenbichler and M. Muhlhauser. «An IR local positioning system for smart items and devices». In: *23rd International Conference on Distributed Computing Systems Workshops, 2003. Proceedings.* 2003, pp. 334–339. DOI: 10.1109/ICDCSW.2003.1203576 (cit. on p. 5).

[6] A. Ward, A. Jones, and A. Hopper. «A new location technique for the active office». In: *IEEE Personal Communications* 4.5 (1997), pp. 42–47. DOI: 10.1109/98.626982 (cit. on p. 5).

[7] J. Krumm, S. Harris, B. Meyers, B. Brumitt, M. Hale, and S. Shafer. «Multi-camera multi-person tracking for EasyLiving». In: *Proceedings Third IEEE International Workshop on Visual Surveillance.* 2000, pp. 3–10. DOI: 10.1109/VS.2000.856852 (cit. on p. 6).

[8] Wenchao Huang, Yan Xiong, Xiang-Yang Li, Hao Lin, Xufei Mao, Panlong Yang, Yunhao Liu, and Xingfu Wang. «Swadloon: Direction Finding and Indoor Localization Using Acoustic Signal by Shaking Smartphones». In: *IEEE Transactions on Mobile Computing* 14.10 (2015), pp. 2145–2157. DOI: 10.1109/TMC.2014.2377717 (cit. on p. 6).

[9] Sverre Holm. «Hybrid ultrasound-RFID indoor positioning: Combining the best of both worlds». In: *2009 IEEE International Conference on RFID*. 2009, pp. 155–162. DOI: 10.1109/RFID.2009.4911169 (cit. on p. 6).

[10] L.M. Ni, Yunhao Liu, Yiu Cho Lau, and A.P. Patil. «LANDMARC: indoor location sensing using active RFID». In: *Proceedings of the First IEEE International Conference on Pervasive Computing and Communications, 2003. (PerCom 2003).* 2003, pp. 407–415. DOI: 10.1109/PERCOM.2003.1192765 (cit. on p. 7).

[11] Thomas King, Stephan Kopf, Thomas Haenselmann, Christian Lubberger, and Wolfgang Effelsberg. «COMPASS: A Probabilistic Indoor Positioning System Based on 802.11 and Digital Compasses». In: *Proceedings of the 1st International Workshop on Wireless Network Testbeds, Experimental Evaluation & Characterization*. WiNTECH '06. Los Angeles, CA, USA: Association for Computing Machinery, 2006, pp. 34–40. ISBN: 1595935398. DOI: 10.1145/1160987.1160995. URL: https://doi.org/10.1145/1160987.1160995 (cit. on p. 7).

[12] Markus Kohne and Jurgen Sieck. «Location-Based Services with iBeacon Technology». In: *2014 2nd International Conference on Artificial Intelligence, Modelling and Simulation*. 2014, pp. 315–321. DOI: 10.1109/AIMS.2014.58 (cit. on p. 7).

[13] Liron David, Avinatan Hassidim, Yossi Matias, Moti Yung, and Alon Ziv. «Eddystone-EID: Secure and Private Infrastructural Protocol for BLE Beacons». In: *IEEE Transactions on Information Forensics and Security* 17 (2022), pp. 3877–3889. DOI: 10.1109/TIFS.2022.3214074 (cit. on p. 7).

[14] S. Gezici, Zhi Tian, G.B. Giannakis, H. Kobayashi, A.F. Molisch, H.V. Poor, and Z. Sahinoglu. «Localization via ultra-wideband radios: a look at positioning aspects for future sensor networks». In: *IEEE Signal Processing Magazine* 22.4 (2005), pp. 70–84. DOI: 10.1109/MSP.2005.1458289 (cit. on p. 8).

[15] S. Gezici, I. Guvenc, and Z. Sahinoglu. «On the Performance of Linear Least-Squares Estimation in Wireless Positioning Systems». In: *2008 IEEE International Conference on Communications*. 2008, pp. 4203–4208. DOI: 10.1109/ICC.2008.789 (cit. on p. 17).